Na/Li substitution effect on the structural, electrical and magnetic properties of LiCr(MoO4)2 and β Li0.87Na0.13Cr(MoO4)2

Manel Sonni, Mohamed Faouzi Zid, El-Kebir Hlil, Kader Zaïdat, Cécile Rossignol, Saïd Obbade

Version of Record: https://www.sciencedirect.com/science/article/pii/S0925838820311038
Manuscript_a21c7fd23a9deb5ae33a34e0a7051877

Na/Li substitution effect on the structural, electrical and magnetic properties of $LiCr(MoO_4)_2$ and β–$Li_{0.87}Na_{0.13}Cr(MoO_4)_2$

Manel Sonni [a, b], Mohamed Faouzi Zid [a], El Kebir Hlil [c],
Kader Zaidat [d] Cécile Rossignol [b] and Saïd Obbade [b, *]

[a] *Laboratory of material, crystallography and applied thermodynamic, faculty of sciences Tunisia.*
[b] *Univ. Grenoble Alpes, Univ. Savoie Mont Blanc, CNRS, Grenoble INP, LEPMI, 38000 Grenoble, France*
[c] *MCBT-UPR CNRS, Néel Institute, Grenoble Alpes University, F-38000 Grenoble, France.*
[d] *SIMAP-UMR CNRS, Univ. Grenoble Alpes, Grenoble INP, F-38000 Grenoble, France.*

Abstract:

The novel bi-molybdate β–$Li_{0.87}Na_{0.13}Cr(MoO_4)_2$ was prepared by solid state reaction route. Single crystal X-ray diffraction experiment revealed that the compound crystallizes in the triclinic system, in P -1 space group with a = 6.715 (2), b = 7.160 (3), c = 7.237 (1) Å, α = 91.16° (3), β = 110.59° (2), γ = 105.54° (3). Its crystal structure is isotypic to $LiCr(MoO_4)_2$ which has interesting magnetic and electrochemical properties **[1-3]**. Bond valence sum (BVS) and charge distribution (CHARDI) validation tools supported the structural model.

The electrical properties were systematically studied by impedance spectroscopy. The ionic conductivity measurements are performed on pellets of 82% and 87% relative density for $LiCr(MoO_4)_2$ and β–$Li_{0.87}Na_{0.13}Cr(MoO_4)_2$ respectively. AC impedance spectroscopy studies show that the highest overall conductivity is $\sigma_{326°C} = 7.86 \times 10^{-7}$ S.cm^{-1}

Probable diffusion pathways of Li^+ ions in the both structures were simulated using the bond valence sum BVS maps method. This analysis shows that the ionic transport in these materials is essentially due to simple hopping of Li^+ ions parallel to (101) plane.

For β–$Li_{0.87}Na_{0.13}Cr(MoO_4)_2$ compound, the *in-situ* High Temperature X-Ray Diffraction (HTXRD), in the temperature range from 25 to 650°C, were also performed and Unit-cell thermal expansion has been discussed.

The magnetic study show that these compounds present an antiferromagnetic order below the temperatures T_N = 16 and 30 K for $LiCr(MoO_4)_2$ and β–$Li_{0.87}Na_{0.13}Cr(MoO_4)_2$ respectively.

Key words: bi-molybdate, crystal-structure, X-ray diffraction, Impedance spectroscopy, ions Pathway simulation, magnetic properties, thermal expansion.

* Corresponding author**: said.obbade@phelma.grenoble-inp.fr**

INTRODUCTION:

In recent years, the properties of high ionic conductivity materials have been extensively studied. In general, the properties of a material are closely related to the crystal structure and tunnel size as well as grain size, shape and dimensionality **[4-6]**. Occupying both tetrahedral and octahedral sites, molybdenum combined with mixed transition metal MO_n polyhedra gives rise to original structures with tunnels and cavities that promote the mobility of alkaline ions in these anionic structures. **[7-10]**. Therefore, structural studies of new polyanionic materials are essential to understand and predict the migration pathways of alkaline ions in these materials **[11]**. According to their structure, molybdates constitute an important class of materials with varied functional properties. Alkali-containing anionic framework structures have attracted great interest in recent decades, mainly for their ionic conductivity properties and their use as batteries electrodes materials. In addition to their use in Li-ion and Na-ion batteries **[3, 12-17]**, molybdates containing alkaline ions and trivalent cations are also interesting for many industrial applications, including solid electrolytes, ferroelectrics, photo-catalysts and optical materials (light-emitting diodes and lasers) **[18-24]**.

For the formula $ACr(MoO_4)_2$ with (A = alkaline metal), only the phase with Lithium $LiCr(MoO_4)_2$ has been synthesized **[1]**. In previous studies, $LiM(MoO_4)_2$ compounds with M =Fe and Cr, were chosen as electrode material for lithium-ion batteries **[3,12]**. Although the $LiCr(MoO_4)_2$, is a known phase, no study of these electrical properties has been performed to date. Its structure and these magnetic properties have been studied **[1, 3]**. Nevertheless, it was interesting to prepare this compound to make a comparison with the new compound β–$Li_{0.87}Na_{0.13}Cr(MoO_4)_2$ under the same conditions.

Thus, in this paper we present in a first section the synthesis and the crystal structure determination from single-crystal X-ray diffraction data of the new phase β–$Na_{0.13}Li_{0.87}Cr(MoO_4)_2$. The proposed structural model is supported by the charge-distribution (CHARDI) analysis **[25–27]** and bond-valence-sum (BVS) **[28, 29]** calculations. The influence of alkaline Li-Na substitution, on the electrical conductivity will be discussed in terms of impedance spectroscopy study and transport pathways of lithium ion simulation accompanied by the correlation between structure and ionic conductivity. A study of particle morphology, the thermal stability, as well as magnetic proprieties of both compounds is also reported.

EXPERIMENTAL SECTION:

For the preparation of this material we ground the reagents $NaNO_3$ (Alfa-Aesar 98.9%), Li_2CO_3 (Sigma-Aldrich 99.0%), Cr_2O_3 (Sigma-Aldrich 99.9%) and $(NH_4)_6Mo_7O_{24}{\cdot}4H_2O$ (Sigma-Aldrich 99.98%) in the ratio Na /Li /Cr /Mo equal to 7 /7 /5/6 using an agate mortar in order to have a reactive and homogeneous mixture; the powder thus obtained was calcined at 400 °C for 12 hours to remove all volatile compounds. After fine grinding, the resulting mixture was heated at 630 °C for 3 days. After a slow cooling (5°C/h) up to 580 °C followed by a fast cooling of 50°C/h up to ambient temperature, purple crystals of parallelepiped shape and optimal size for data collection, have been obtained.

A good quality single crystal selected under a polarizing microscope has been glued to a Lindemann glass then used for the determination of the first crystallographic parameters. The search and refinement of 25 intense reflections obtained by a Enraf-Nonius CAD-4 four-circle diffractometer equipped with a monochromatic Mo-Kα radiation (0.71069 Å), made it possible to select the crystalline system as well the cell parameters. The crystallographic characteristics found are detailed in **Table S1** (See **S**upplementary Materials). An examination of the structural data found in the various databases shows that the cell parameters obtained are related to those of the $LiCr(MoO_4)_2$ compound **[1]**. The chosen crystal served therefore for the collection of diffracted intensities. The conditions of the measurements are summarized in **Table S2**.

As to structural validation tools, Bond Valence Sum BVS **[28, 29]** and Charge Distribution analysis CHARDI **[25–27]** were used to validate the structural model. The CHARDI and BVS computations have been obtained with the CHARDI-IT **[26]** and SoftBV **[28]** programs, respectively.

In order to have available enough amount for characterization by several techniques, especially the impedance spectroscopy, we have also prepared powder samples of both $LiCr(MoO_4)_2$ and β–$Li_{0.87}Na_{0.13}Cr(MoO_4)_2$ compounds by autocombustion method using nitrate salts as oxidizers and glycine acid as fuel and complexing agent. Stoichiometric proportions of $LiNO_3$, $NaNO_3$, $Cr(NO_3)_3{\cdot}9H_2O$ and $(NH_4)_6Mo_7O_{24}{\cdot}4H_2O$ were completely dissolved in a solution of glycine acid $C_2H_5NO_2$. The molar ratio of glycine to nitrate amounts was kept constant at 0.4. During the first synthesis step, the excess water was evaporated by heating at 110°C. Throughout this evaporation stage, viscous liquid foams were observed before the obtaining of fine particles as a result of a very fast auto-ignition. To clear the remaining organic residues, the obtained powder was then put in the oven at 300°C overnight, then in a tubular furnace at 650°C for 24 hours to obtain a pure phase.

The purity of powders thus prepared was verified by powder X-ray diffraction. The powder XRD data for phases identification were collected at ambient temperature on a D8 Bruker

diffractometer using Cu Kα radiation ($\lambda_{Cu}K\alpha$=1.54056 Å). The measurement was performed under Bragg–Brentano geometry at 2θ with step 0.017° in the range extended from 10° to 80°.

Thermal analyses (TGA/DTA) were performed under air flow using a SETARAM TAG24-16 thermal analyzer. Thermal measurements were carried out on sample placed in a platinum crucible in a temperature range from room temperature to 1000 °C with a speed of 5 °C min^{-1}.

Impedance spectroscopy measurements were carried out using a Hewlett-Packard 4192a Impedance Analyzer. The impedance spectra were recorded in the 5 Hz-13 MHz frequency range with 0.3V rms ac signal. A pellet was prepared by uniaxial shaping followed by isostatic pressing at 2.5 Kbar and sintering at 700 °C for 3h in air with 5 °min^{-1} heating and cooling rates. After these treatments, the samples achieved 82% and 87% of the theoretical density for $LiCr(MoO_4)_2$ and β–$Li_{0.87}Na_{0.13}Cr(MoO_4)_2$, respectively. A layer of gold paste was deposited on both faces of the pellet using a SC7620 Metallizer to ensure good electric contacts. Before and after sintering, the microstructure of the pellets was analyzed using a JEOL IT500HR LV microscope.

Bond Valence Energy Landscape "BVEL" calculations were performed using the 3DBVSMAPPER code using Li^+ as a test ion and default settings **[30]**. The BVEL isosurfaces were visualized and represented using the VESTA3 program **[31]**.

Bond valences "$s_{A\text{-}X} = \exp[(R_0 - R_{A\text{-}X}) / b]$" for the interaction between an anion X and a cation A, also their mismatches are primarily expressed randomly "valence units". Recently, it was shown that they may be also related to an absolute energy scale by expressing the bond valence as a Morse-type interaction energy **[32-34]**. For details, see **[33]**. Briefly, the pathway approach defines regions with low energy *E(A)* :

$$E(A) = D_0 \left[\sum_{i=1}^{N} \left(\frac{s_{A-X_i} - s_{min,A-X_i}}{s_{min,A-X_i}} \right)^2 - N \right] + \sum_{i=1}^{N} E_{Coulomb}\,(A-B) \qquad (1)$$

with

$$E_{Coulomb}(A-B) = 14.4\ \frac{eV}{\text{Å}}\ \frac{z_A . z_B}{R_{A-B}}\ erfc\left(\frac{R_{A-B}}{\rho_0}\right) \qquad (2)$$

The fractional ion charges z_A and z_B are derived from the nominal charges and principal quantum numbers by the formalism explained in **[33, 34]**. Coulomb attraction terms are generally integrated in the Morse attraction term. The activation energy required for the migration of a cation from a site A to a site B is the difference between the site energy (B) and the site energy (A): $E_a = E(B) - E(A)$.

In situ high-temperature X-ray diffraction (HTXRD) experiments were also performed under dynamic air (5 L h^{-1}) in an Anton Paar HTK1200N chamber equipped with an automatic compensation of dilation according to Z axis, of PANalytical X'Pert Pro MPD diffractometer (in θ/θ

mode and with Cu-anode X-ray tube Kα1 = 1.54056 Å, Kα2 = 1.54439 Å) equipped with a 1D X'Celerator detector. Several diagrams were recorded in air between ambient temperature and 650°C every 25 °C, in the range 10–70°(2θ), with a step of 0.017°and heating at 0.8 °C min^{-1}.

The magnetic measurements of the as prepared samples were also carried out using the commercial Physical Properties Measurements System device (Quantum Design, PPMS), and magnetization M(T) was measured versus temperature ranging from 2 to 400 K, under an external magnetic field of 0.05 T. The field dependence of the magnetization M (H) was measured at 2 K by varying the applied magnetic field between -6 and 6 T.

RESULTS AND DISCUSSION

Crystal structure determination

Crystal structure refinement of β–$Li_{0.87}Na_{0.13}Cr(MoO_4)_2$

After single crystal X-ray diffraction data processing by the Wingx chain **[35]**, an empirical absorption correction by psi-scan was performed **[36],** and crystal structure was solved in the centrosymmetric *P-1* space group by means of a direct methods strategy that localizes the heavy atoms Mo and Cr, followed by a Fourier-difference maps examination to localize light atoms Na, O and Li, respectively. At the end of the resolution of the structure, we observe that the alkaline-oxygen distance A-O is a little higher than that of Li-O encountered in the literature **[1, 9]**. It is therefore an average between those of Na-O and Li-O. At this level the use of the EADP, EXYZ and SUMP constraints allowed by the SHELXL-97 program **[37]** were applied. The refinement leads to the occupancy rates grouped in **Table S3**. At the end of the crystal structure refinement, a last Fourier-difference examination reveals no significant peak and the remaining maximum and minimum electron densities are acceptable. In addition, the final refinement leads to well-defined ellipsoids for all atoms. **Table S4** summarizes the results of the refinement. The reduced atomic coordinates and the thermal stirring factors are reported in **Table S3**.

The geometric parameters of the various coordination polyhedra are presented in **Table 1 and Table S5**. CCDC 1957397, contains the supplementary crystallographic data for and β–$Li_{0.87}Na_{0.13}Cr(MoO_4)_2$ compound.

Table 1: Main interatomic distances (Å) and angles (°) in the coordination polyhedra for β–$Li_{0.87}Na_{0.13}Cr(MoO_4)_2$.

Mo1			
Mo1—O6	1.697 (3)	Mo1—O8^{i}	1.861 (2)
Mo1—O5	1.707 (3)	Mo1—O7	1.878 (2)
Mo1—O8	2.481(2)	Mo1—O4	2.635 (9)
Mo2			
Mo2—O4	1.736 (3)	Mo2—O2	1.780 (2)
Mo2—O3	1.756 (2)	Mo2—O1	1.790 (2)

Cr1			
Cr—O7^{v}	1.940 (2)	Cr—O7	1.966 (2)
Cr—O3^{vi}	1.947 (3)	Cr—O2^{vii}	1.973 (2)
Cr—O8	1.952 (2)	Cr—O1^{v}	1.973 (2)
NaLi			
NaLi—O5	1.999 (5)	NaLi—O8^{iii}	2.177 (5)
NaLi—O4^{viii}	2.117 (5)	NaLi—O1^{x}	2.223 (5)
NaLi—O6^{ix}	2.144 (6)	NaLi—O5^{iii}	2.699 (6)

Symmetry codes : (i) −*x*+2, −*y*+1, −*z*+1; (ii) *x*+1, *y*, *z*; (iii) −*x*+1, −*y*+1, −*z*+1; (iv) *x*+1, *y*+1, *z*; (v) −*x*+2, −*y*+2, −*z*+1; (vi) *x*, *y*, *z*+1; (vii) −*x*+3, −*y*+2, −*z*+1; (viii) *x*−1, *y*, *z*; (ix) −*x*+1, −*y*+1, −*z*; (x) *x*−1, *y*−1, *z*; (xi) *x*, *y*, *z*−1.

Crystal structure description of β–$Li_{0.87}Na_{0.13}Cr(MoO_4)_2$

β-$Na_{0.13}Li_{0.87}Cr(MoO_4)_2$ compound crystallize in the same structure that $LiCr(MoO_4)_2$ with a one mixed alkaline crystallographic site, where Li^+ and Na^+ cations are localized in the tunnels formed by three-dimensional framework obtained by association of transition metals (Mo and Cr) polyhedrons. The two independent Molybdenum atoms are bonded by four oxygen atoms at short distances from 1.697 to 1.878 and 1.736 to 1.790 Å for Mo(1) and Mo(2), respectively, to form tetrahedral environment MoO_4, **Figure S1**. The Mo(1) tetrahedron can be completed by two large oxygen distances (Mo1-O8 = 2.481 Å) and (Mo1-O4 = 2.634 Å) to form an very distorted $Mo(1)O_6$ octahedral coordination, **Figure S1**. The chromium atoms adopt a single octahedral environment, **Figure 1**.

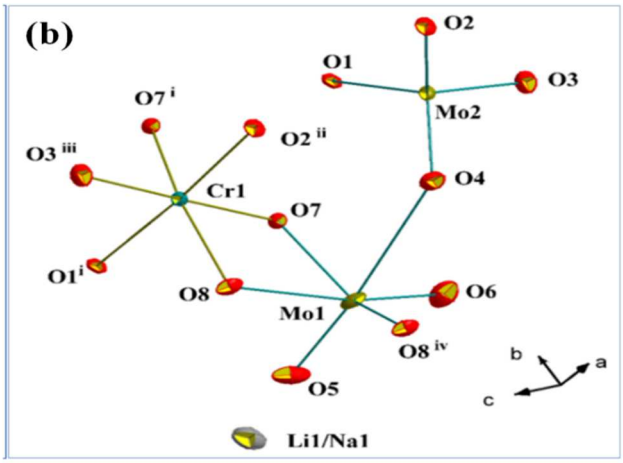

Fig.1: The structural unit of β–$Li_{0.87}Na_{0.13}Cr(MoO_4)_2$,
(a) with tetrahedral $Mo(1)O_4$ and (b) octahedral $Mo(1)O_6$, environments.
Symmetry code: (i): 2-x, 2-y, 1-z; (ii): 3-x, 2-y, 1-z, (iii) : x, y, 1+z, (iv) : 2-x, 1-y, 1-z.

Thus, structural unit of the β–$Li_{0.87}Na_{0.13}Cr(MoO_4)_2$ compound consists of a $Mo(1)O_6$ octahedra sharing corner O(4) with $Mo(2)O_4$ tetrahedron and O(7) O(8) edge with the $Cr(1)O_6$ octahedron, to form a trimeric unit $[Mo_2CrO_{13}]^{11-}$, **Figure 1**. Each octahedron $Cr(1)O_6$ and $Mo(1)O_6$ is linked by edge to an identical polyhedron to form two dimeric units $[Cr_2O_{10}]^{14-}$ and $[Mo(1)_2O_{10}]^{8-}$, respectively. Those units share edges between them to build an infinite chain $[Cr_2Mo_2O_{16}]_{\infty}^{14-}$ along the ***b*** axis, **Figure 2a**. This infinite chain can become $[Cr_2Mo_2O_{14}]_{\infty}^{10-}$ if we consider molybdenum Mo(1) in tetrahedral coordination, **Figure 2b**.

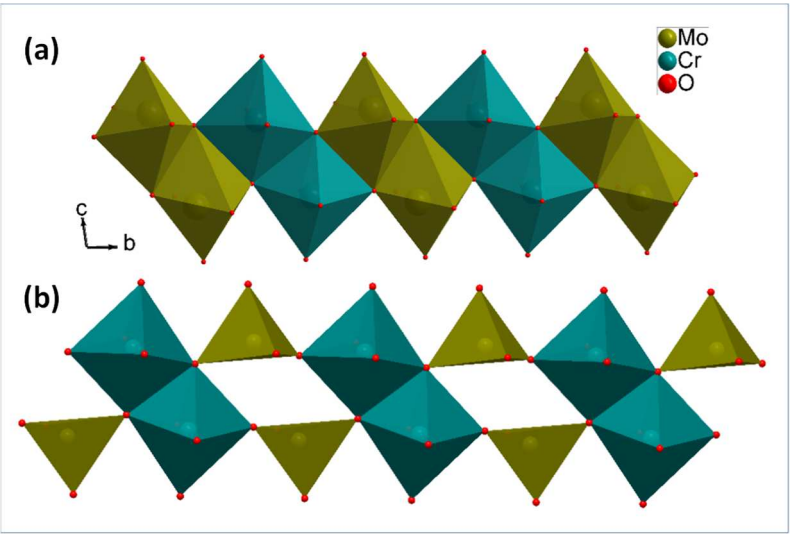

Fig. 2: Difference between (a) $[Cr_2Mo_2O_{16}]_\infty^{14-}$ and (b) $[Cr_2Mo_2O_{14}]_\infty^{10-}$ infinite chains.

Two adjacent infinite chains $[Cr_2Mo_2O_{16}]_\infty^{14-}$ are linked together by Mo(1)─O─Mo(2) and Cr(1)─O─Mo(2) mixed bridges, to form a three-dimensional anionic framework leaving free tunnels along [101] direction, in which the alkaline cations Li^+ and Na^+ are localized **(Figure 3)**.

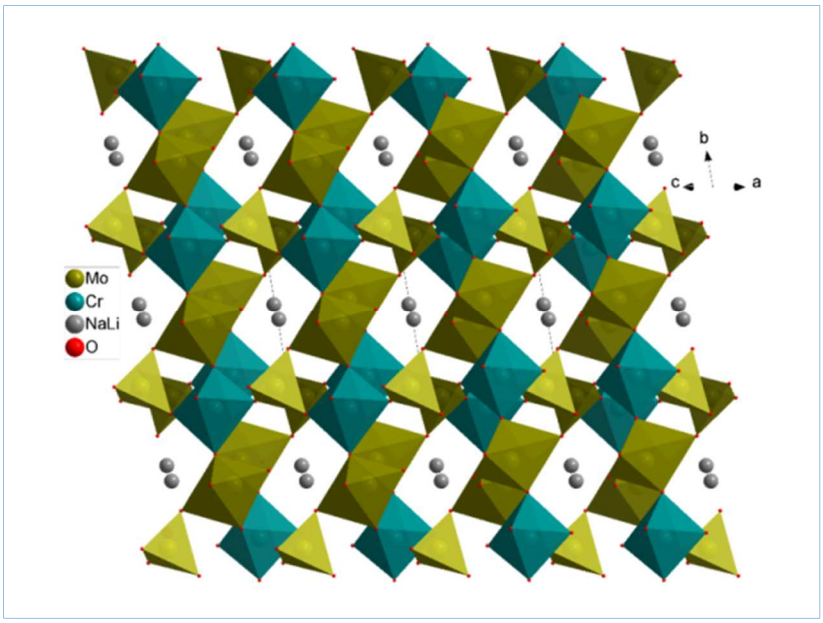

Fig. 3: Presentation of the structure of β–$Li_{0.87}Na_{0.13}Cr(MoO_4)_2$ in the direction [101].

An examination of different structures found in the literature reveals that the compounds of general formula $A^IM^{III}(MoO_4)_2$ have a structural diversity. In fact, the structures of the molybdates $CsFe(MoO_4)_2$ **[38]** and $NaFe(MoO_4)_2$ **[39]** having as space group P-3m or C2/c, respectively, adopt the same types of layers where molybdenum atom occupies only the tetrahedral sites (**Figure S2**).

CHARDI and Bond Valence Sums (BVS) validation

The proposed structural model, particularly the distribution at alkaline site A1 (Li/Na), is well confirmed by the two validation models: the sum of the BVS link valences and the CHARDI charge distribution method.

Table 2: CHARDI and BVS analysis of the cations in the compound β–$Li_{0.87}Na_{0.13}Cr(MoO_4)_2$.

Cation	$q(i)\cdot sof(i)$	$Q(i)$	$V(i)$	CN(i)	ECoN(i)	d_{moy}	d_{med}
Mo1	6.000	-	6.0886	6	-	2.0430	2.0431
	6.000	5.790	5,6988	4	3.67	1.7856	1.7856
Mo2	6.000	6.150	5.9770	4	3.98	1.7652	1.7652
Cr	3.00	3.060	3.0963	6	5.99	1.9585	1.9584
A(Li1/Na1)	1.000	1.000	1.0208	6	4.88	2.2264	2.2263

Moreover, a rigorous examination of the calculation results given in Table 6 shows that the calculated charge values Q(i) and valences V(i) are in good agreement with the oxidation levels weighted by the occupancy rates. Bond valence sums calculation provides values of 6.089, 5.977, 3.004 and 1.021 *v.u.* for Mo(1), Mo(2), Cr and mixed Li/Na site, respectively, which are consistent with formal valences Mo^{6+} Cr^{6+} and (Li^{+}/Na^{+}). Thus, observed distortion of $Mo(1)O_6$ and $(Li/Na)O_6$ octahedrons, has no remarkable effect on the average distances nor on the charges of the ions in the structures which prove to be identical to those recorded in **Table 2** and similar to those encountered in different molybdates of the literature **[1, 7-11]**.

Powder X-ray diffraction of β-$Na_{0.13}Li_{0.87}Cr(MoO_4)_2$ and $LiCr(MoO_4)_2$

The refinement of the diffractograms was carried out, using the Fullprof program **[40]**, by the Le Bail method **[41]**, which consists in refining only the parameters of profile and unit-cell. During profile matching, the background is likened to a polynomial equation and the line profile to a pseudo-Voight equation. When all these parameters are refined as well as the cell parameters and zero, a good superposition is obtained between the experimental diffractograms and the refined one (**Figures 4 and 5**). The refined crystallographic and profile Matching parameters are given in **Table 3**.

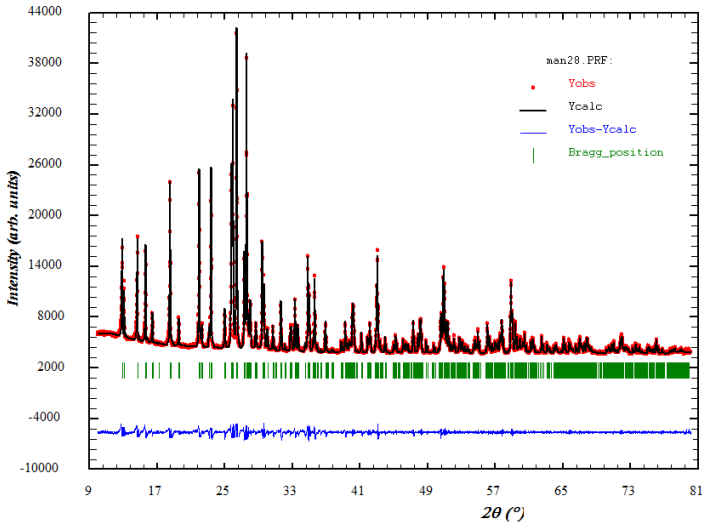

Fig. 4: Profile Matching result of β–$Li_{0.87}Na_{0.13}Cr(MoO_4)_2$.

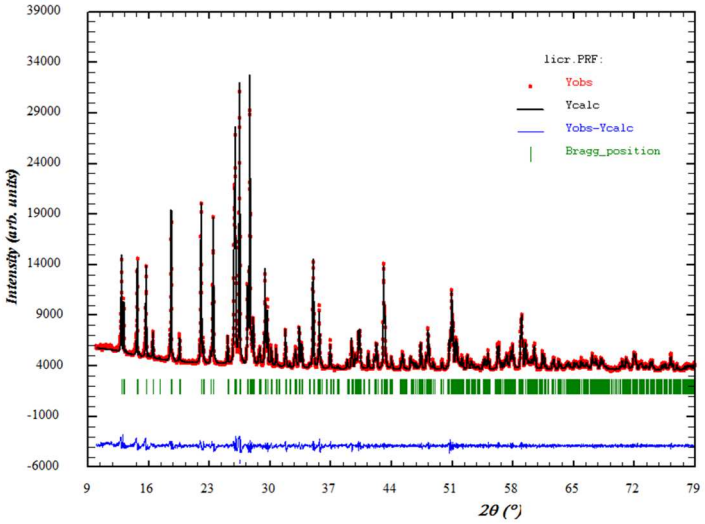

Fig. 5: Profile Matching result of $LiCr(MoO_4)_2$.

Table 3: Crystallographic data of the indexed phases and the matching profile factors.

Compound	β–$Li_{0.87}Na_{0.13}Cr(MoO_4)_2$.	$LiCr(MoO_4)_2$
Crystallographic data		
Crystal system	Triclinic	Triclinic
Space group	P -1	P -1
Cell parameters	a= 6.7236Å, b= 7.1718Å, c=7.2487Å, α= 91.176°,β=110.545°,γ=105.579°	a=6.7090Å, b=7.1629Å, c=7.2323Å, α=91.094°, β=110.4139°, γ=105.5128°
Volume (Å³)	312.934	310.840
Refinement results		
R_p %	2.66	2.26
R_{wp} %	4.13	3.18
R_{exp} %	1.41	1.44
Number of refined parameters	36	36

Thermal Analysis of β–$Li_{0.87}Na_{0.13}Cr(MoO_4)_2$

The thermal analysis curves of β–$Li_{0.87}Na_{0.13}Cr(MoO_4)_2$, performed in the thermal range from room temperature to 1000°C are shown in **Figure S3**. In the heating cycle, no significant weight loss has been observed up to incongruent melting point at about 810°C, indicated by an endothermic peak in DTA curve. The very minor weight loss, on the order of 1%, can be attributed to small errors associated with a potential evaporation of a small amount of surface moisture. While cooling the sample, three exothermic peaks are observed, which are characteristic of the crystallization of the phases formed after decomposition of the compound during the non-congruent melting phase.

Morphological Properties

We present in **Figures 6a, 8b, 8c and 8d** the lozenge morphologies of $LiCr(MoO_4)_2$ and β–$Li_{0.87}Na_{0.13}Cr(MoO_4)_2$ before and after sintering respectively. We observe grains of similar sizes to those of un-sintered pellets and large grains resulting from the agglomeration of several grains.

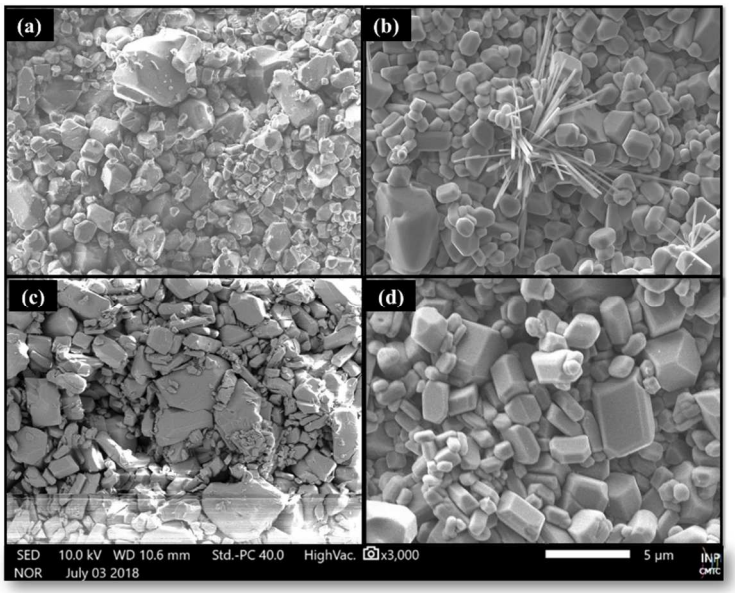

Fig. 6: SEM micrographs of pellets; $LiCr(MoO_4)_2$; (a): before sintering, (b): after sintering and β–$Li_{0.87}Na_{0.13}Cr(MoO_4)_2$; (c): before sintering, (d): after sintering.

Electrical Properties

Impedance Spectra

To evidence eventual alkali cations mobility in the channels occupied by Li^+ and Na^+ along [101] direction, ionic conductivity measurements were carried out. The Nyquist plots of $LiCr(MoO_4)_2$ and β–$Li_{0.87}Na_{0.13}Cr(MoO_4)_2$ samples, at different temperatures, are thus shown in **Figure 7, Figure S4** and **Figure 8,** respectively. Zview software **[42]** was used to fit plots. It can be noted that in high frequency domain, the impedance diagrams show only one typical semicircle arc. Thus, an equivalent circuit containing a resistor R connected in parallel with a constant phase element CPE has been used to adjust the impedance diagrams. The latter contribution is an empirical impedance function of the type: $Z_{(CPE)} = \frac{1}{A(j\omega)^p}$; (-1 ≤ p≤1), where A is a pseudo capacitance obtained from CPE.

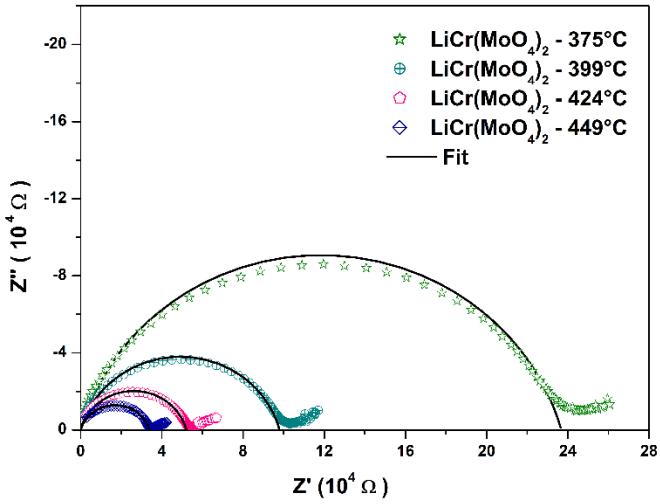

Fig. 7: Complex impedance spectra of $LiCr(MoO_4)_2$ [375°C-449°C].

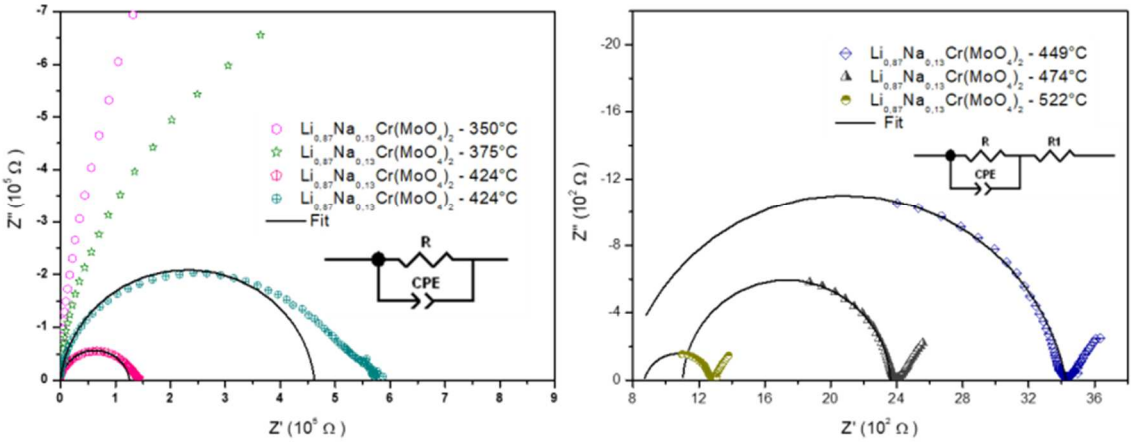

Fig. 8: Complex impedance spectra and equivalent circuits of β–$Li_{0.87}Na_{0.13}Cr(MoO_4)_2$.

At higher temperatures, the impedance spectra are shifted from their origin. This led us to add to the previous circuit a resistor R_1 in series taking into account the contacts of the electrodes and external wires. The fitted values of different electric parameters for $LiCr(MoO_4)_2$ and β–$Li_{0.87}Na_{0.13}Cr(MoO_4)_2$ compounds, at different temperatures, are illustrated in **Table 4** and **5**. Note that, at low frequencies (f ≤ 20Hz), a minor contribution is spotted; it is tentatively assigned to interfacial phenomena related to the electrode reaction **[43]**, and not investigated further.

Table 4: Electrical parameters of $LiCr(MoO_4)_2$ obtained from equivalent circuits at 326 ≤T(°C) ≤618, refined using Z-view software.

T(°C)	$R_1(\Omega)$	$R(\Omega)$	$A(10^{-11}\ Fs^{p-1})$	p	$C(10^{-12}\ F)$	$\sigma_{dc}(S\ cm^{-1})$
326	-	975700	2.82	0.83625	3.61	$7.864\ 10^{-7}$
350	-	477550	2.92	0.83749	3.34	$1.607\ 10^{-6}$
375	-	236760	3.34	0.83241	3.14	$3.241\ 10^{-6}$
399	-	97954	3.06	0.84024	2.73	$7.833\ 10^{-6}$
424	-	52078	3.13	0.84201	2.57	$1.473\ 10^{-5}$
449	-	33948	4.41	0.82556	2.59	$2.260\ 10^{-5}$
474	-	22291	4.94	0.82169	2.52	$3.442\ 10^{-5}$
496	-	14897	5.96	0.81312	2.42	$5.151\ 10^{-5}$
522	-	9933	6.64	0.80912	2.31	$7.725\ 10^{-5}$
547	-	6451	8.66	0.79616	2.17	$1.189\ 10^{-4}$
595	1328	1321	3.23	0.93592	10.12	$5.808\ 10^{-4}$
618	1284	645.2	2.54	0.99614	23.66	$1.189\ 10^{-3}$

Table 5: Electrical parameters of β–$Li_{0.87}Na_{0.13}Cr(MoO_4)_2$ obtained from equivalent circuits at 399≤θ (°C) ≤522, refined using Z-view software.

T(°C)	$R_1(\Omega)$	$R(\Omega)$	$A(10^{-11}\ Fs^{p-1})$	p	$C(10^{-12}\ F)$	$\sigma_{dc}(S\ cm^{-1})$
399	-	462060	0.49	0.93671	2.05	$1.617\ 10^{-6}$
424	-	125460	0.56	0.93269	2.03	$5.954\ 10^{-6}$
449	741,4	2686	3.72	0.87475	3.69	$2.781\ 10^{-4}$
474	1102	1260	1.68	0.96451	8.75	$5.928\ 10^{-4}$
522	868	409	45.6	0.8359	21.77	$1.826\ 10^{-3}$

In the linear Arrhenius plot for total alkaline ions conductivity [$\ln(\sigma_{dc}T)$ *vs.* 1000/T], given in **Figure 9**, two regions with distinctly different slopes can be seen, with a crossover occurring around 430°C for β–$Li_{0.87}Na_{0.13}Cr(MoO_4)_2$ sample. For both compounds the temperature-dependent ionic conductivity increases from $7.86.10^{-7}$ S cm^{-1} at 326°C to $1.19.10^{-3}$ S cm^{-1} at 618°C for $LiCr(MoO_4)_2$ and from $1.62.10^{-6}$ S cm^{-1} at 399°C to $1.83.10^{-3}$ S cm^{-1} at 522°C for β–$Li_{0.87}Na_{0.13}Cr(MoO_4)_2$, indicating good ionic conductivities at higher temperatures.

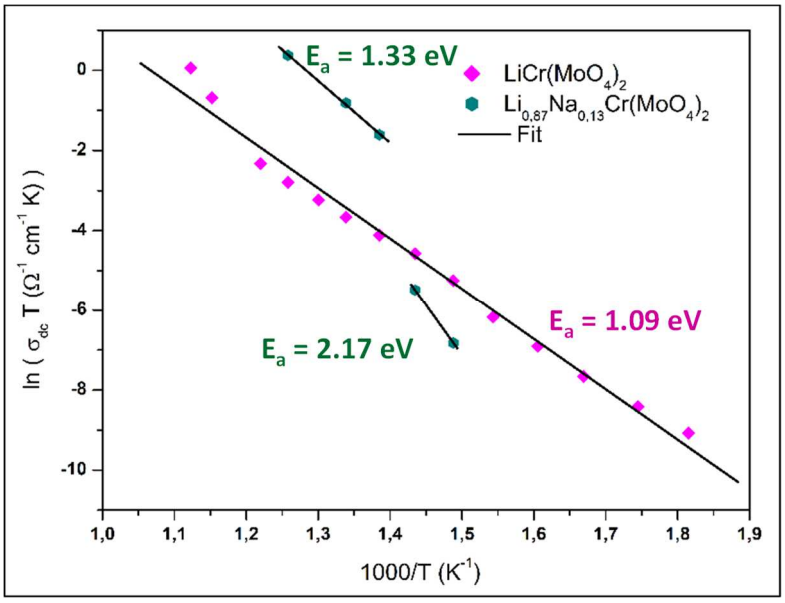

Fig. 9: Arrhenius plot of $LiCr(MoO_4)_2$ and β–$Li_{0.87}Na_{0.13}Cr(MoO_4)_2$ as function of temperature.

Following the Arrhenius law, an activation energy of 1.09 eV is found by fitting data in all thermal range for $LiCr(MoO_4)_2$, while for β–$Li_{0.87}Na_{0.13}Cr(MoO_4)_2$ two different activation energies are found; 2.17 eV between 399 °C and 430 °C, and 1.33 eV in the range of 450 to 522°C. This observation of two distinct linear regions in the Arrhenius plot of β–$Li_{0.87}Na_{0.13}Cr(MoO_4)_2$ sample is common, and generally indicates competition between two or more diffusion mechanisms or a phase transition **[44-48]**.

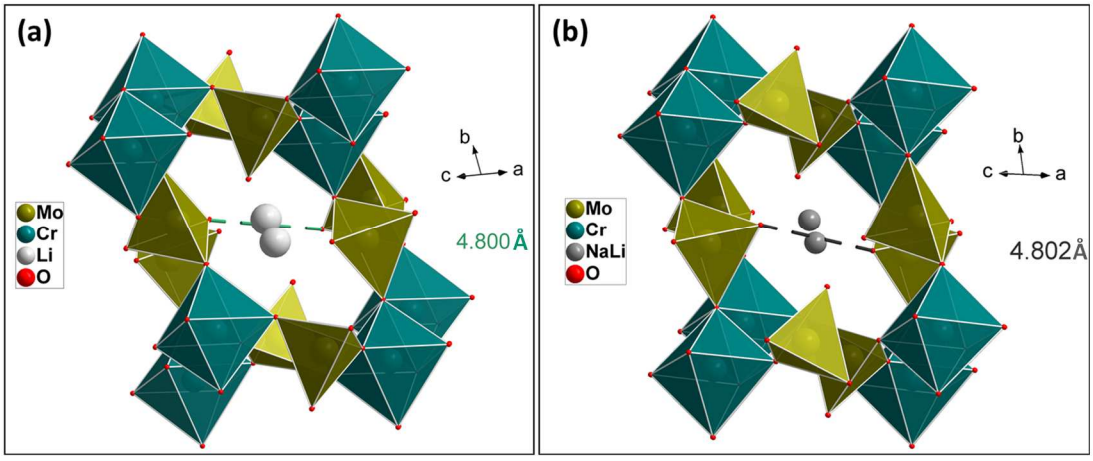

Fig. 10: Tunnels dimensions in (a) $LiCr(MoO_4)_2$ and (b) β–$Li_{0.87}Na_{0.13}Cr(MoO_4)_2$ compounds

To verify if the decrease of conductivity and increase of activation energy, observed at low temperature in β–$Li_{0.87}Na_{0.13}Cr(MoO_4)_2$ compound, is not the result of a steric effect due to the presence of Na^+ cations in tunnels, tunnels dimensions have been examined for both compounds and presented in **Figure 10**. It can be noticed that the partial substitution of the Li site by Na did not result any change in the sections of the tunnels occupied by alkaline cations, with tunnel widths of about 4.80Å for $LiCr(MoO_4)_2$ and 4.802 Å for β–$Li_{0.87}Na_{0.13}Cr(MoO_4)_2$, as shown in **Figure 10a and 10b**, respectively.

However, despite the fact that β–$Li_{0.87}Na_{0.13}Cr(MoO_4)_2$ compound requires a higher activation energy for alkaline cations mobility at low temperature, its conductivity is much higher than $LiCr(MoO_4)_2$ for high temperatures, which shows that the presence of Na cations promotes the improvement of the ionic conductivity in β–$Na_{0.13}Li_{0.87}Cr(MoO_4)_2$ material compared to that of $LiCr(MoO_4)_2$, as it's presented below in the **Tables 4 and 5**.

Pathways transport simulation: Bond Valence Energy Landscape (BVEL) concept

To correlate the structural characteristics of both materials and their ionic conductivity, we have studied the most probable paths of cation migration by the BVEL calculation concept. As expected by crystal structure, the migration of the alkali-ions is according to the direction [101] for both compounds. The activation energies calculated by the program, for the alkali-cations mobility along this direction, are of 1.09 eV for $LiCr(MoO_4)_2$ and 1.49 eV for β–$Li_{0.87}Na_{0.13}Cr(MoO_4)_2$. Thus, the mobility of the alkaline atoms in mixed Li/Na site is more difficult in β–$Li_{0.87}Na_{0.13}Cr(MoO_4)_2$; it encounters more energy barriers than $LiCr(MoO_4)_2$, **Figure 11**.

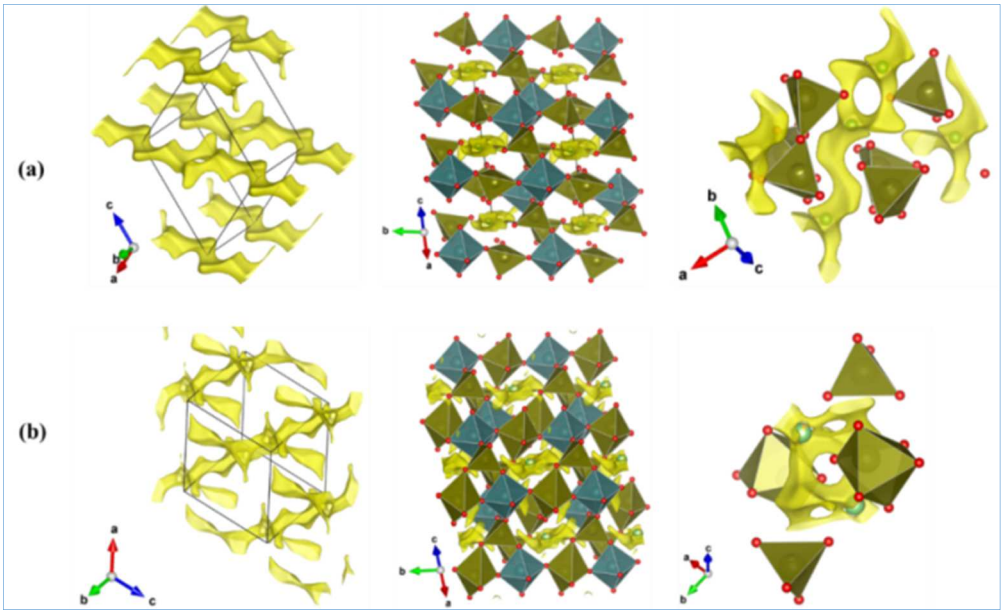

Fig. 11: Bond Valence Energy Landscape of (a) $LiCr(MoO_4)_2$ and (b) β–$Li_{0.87}Na_{0.13}Cr(MoO_4)_2$.

To try to understand the diffusion mechanism as well as to determine the migration paths of alkaline cations in the structure of β–$Li_{0.87}Na_{0.13}Cr(MoO_4)_2$ compound at low temperature. We

determined the isosurfaces of diffusion using an energy value of 2.2 eV, corresponding to the activation energy found for β–$Li_{0.87}Na_{0.13}Cr(MoO_4)_2$ compound (Ea = 2.17 eV, **Figure 9**).

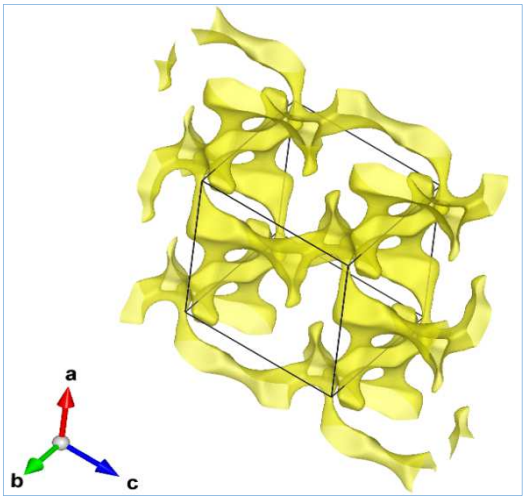

Fig. 12: Bond Valence Energy Landscape of Na^+/Li^+ migration in β–$Li_{0.87}Na_{0.13}Cr(MoO_4)_2$ compound, for energy value of 2.2 eV.

Thus, determination of diffusion isosurfaces, presented in **Figure 12**, shows that the mobility of alkaline ions is along the three crystalline network directions of the structure. This may be explained by the fact that low temperatures do not sufficiently activate the movement of atoms in the network; consequently, ion migration is more difficult.

In-situ High-Temperature X-ray Diffraction

Structural stability and thermal expansion

To complete structural study as well to follow structure thermal stability of β–$Li_{0.87}Na_{0.13}Cr(MoO_4)_2$ compound, the powder High-Temperature X-Ray Diffraction (PHTXRD) has been also done in temperature range of 25 to 650°C. Thus, different diffractograms presented in the **Figure S5** indicate that the β–$Li_{0.87}Na_{0.13}Cr(MoO_4)_2$ phase maintains the triclinic structure and is also structurally stable up to 650°C.

In **Figure 13**, presenting the zoom of the diffractograms in the thermal zone between 430 and 570°C, where the conductivity jump was observed (figure 11), no phase transition was observed confirming the results obtained with DTA-TGA measurements.

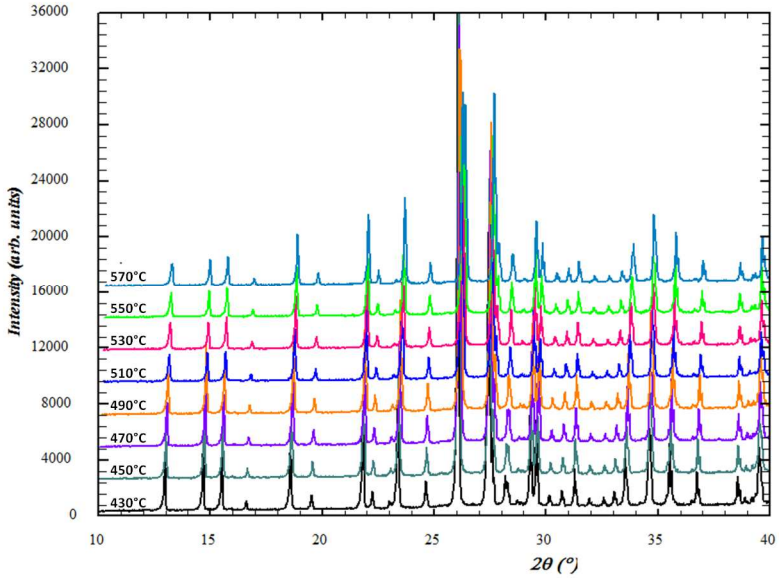

Fig. 13: Powder High-Temperature X-ray Diffraction patterns of β–$Li_{0.87}Na_{0.13}Cr(MoO_4)_2$ for 430°C ≤ T ≤ 570°C

For all temperature, the unit-cell parameters were refined in triclinic symmetry, using the pattern-matching option of Fullprof program and refined unit-cell parameters are listed in **Table S6** and plotted in **Figure S6**.

The plots of thermal evolution of unit-cell parameters and angles presented in **Figure S6**, show that the lattice constants a, c and angles α, β increase upon heating, while b and γ decrease with increasing temperature. The thermal variation of unit-cell parameters (a, b, c), angles (α, β, γ) and volume *V* were followed to fit the binomial equation : $X_T = x_0 + x_1\ T + x_2\ T^2$, with (X= a, b, c, α, β, γ or *V*), where T is the absolute temperature, and (x_0, x_1, x_2) refined coefficients, presented in the **Table 6**.

Table 6: Refined coefficients in binomial equation ($X_T = x_0 + x_1\ T + x_2\ T^2$) of unit-cell thermal variation in β–$Li_{0.87}Na_{0.13}Cr(MoO_4)_2$ compound

	a	**b**	**c**	**α**	**β**	**γ**	***V***
x_0	6.72	7.17	7.24	91.16	110.53	105.63	312.43
x_1 (10^{-5})	5.06	-11.64	38.98	93.34	74.88	196.46	1517.6
x_2 (10^{-8})	2.30	8.14	-10.91	-29.61	14.04	28.34	-78.08

For each temperature, thermal expansion of unit-cell parameters, angles and volume, are determined; where thermal expansion coefficients $\alpha(x)_T$ are defined as $\alpha(x)_T = \frac{1}{x_{273}}\left(\frac{x_T - x_{273}}{T-273}\right)$, with (x= a, b, c, α, β, γ or *V*). Thus, averaged thermal expansion coefficients for crystallographic axes (α_a, α_b, α_c), angles (α_α, α_β, α_γ) and volume α_V are listed in the **Table 7**.

Table 7: The averaged thermal expansion coefficients in the unit cell of β–$Li_{0.87}Na_{0.13}Cr(MoO_4)_2$.

	α_a	α_b	α_c	α_α	α_β	α_γ	α_V
(10^{-6} K^{-1})	9.45	-11.10	47.80	8.72	7.27	-17.40	48.20

The anisotropy of the axial and angular thermal expansivities of (a, c) axes and (α, β) angles; and contractivities of b axis and γ with the magnitude of ($\alpha_c > \alpha_b > \alpha_b$) for unit-cell axes and of ($\alpha_\alpha > \alpha_\beta > \alpha_\gamma$) for angles, accompanied by dramatically decreasing of γ angle (between a and c axes) result in important deformation of metallic polyhedra.

Magnetic Properties

The magnetic behavior for $LiCr(MoO_4)_2$ and β–$Li_{0.87}Na_{0.13}Cr(MoO_4)_2$ compounds has been also studied. Thus, **Figure 14** shows the corresponding temperature dependence of the magnetic susceptibility $\chi(T)$ and his invers χ^{-1}, measured in field-cooled condition under an external magnetic field of 500 Oe, revealing magnetic ordering with an antiferromagnetic component below the Néel temperature T_N.

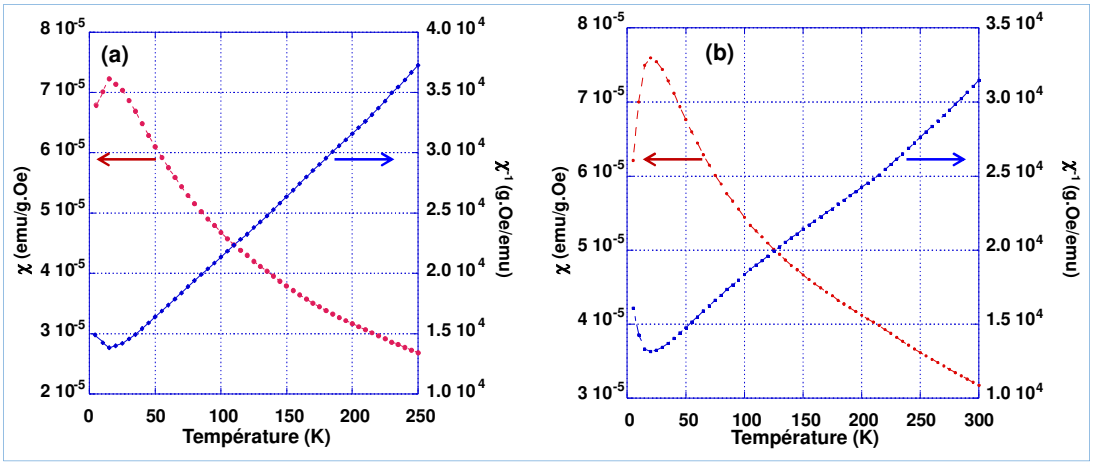

Fig. 14: Magnetic susceptibility χ and inverse χ^{-1} versus temperature from 2 to 300K for (a) $LiCr(MoO_4)_2$ and (b) β–$Li_{0.87}Na_{0.13}Cr(MoO_4)_2$.

Both compounds show a sharp antiferromagnetic (AFM) to paramagnetic (PM) transition with Néel temperature T_N, defined as the temperature corresponding to maximum of the magnetic susceptibility $\chi(T)$ curve, which is about 16K and 30K for $LiCr(MoO_4)_2$ and β–$Li_{0.87}Na_{0.13}Cr(MoO_4)_2$, respectively. The temperature dependence of inverse magnetic susceptibility (χ^{-1}) in the high-temperature range obeys the Curie-Weiss law. Thus, magnetic parameters of the both compounds have been determined by the adjustment of experimental data using a linear law of the inverse susceptibility χ^{-1}; and given in **Table 8**. In addition, it can be seen that the minimums of the χ^{-1} curves are accompanied by negative θ (K) values thus indicating the presence of strong antiferromagnetic couplings. In addition, It is noted that the values of the μ_{eff} obtained experimentally are very close to the theoretical value, 3.87μ_B, calculated for a free Cr^{3+} ($\mu_{eff} = 2\sqrt{S(S+1)}\mu_B$ with S = 3/2).

Table 8: Magnetic characteristics of the compounds $LiCr(MoO_4)_2$ and β–$Li_{0.87}Na_{0.13}Cr(MoO_4)_2$.

Compound	T_N(K)	θ(K)	C	μ_{eff}
$LiCr(MoO_4)_2$	16	-106	1.83	3.88
β-$Li_{0.87}Na_{0.13}Cr(MoO_4)_2$	30	-165	2.23	4.22

To clarify the nature of the transition below Néel temperature T_N, Magnetic isotherms (*M vs H*) were measured at 2K. Magnetic hysteresis M (H) loops for representative samples in antiferromagnetic region from -6T to 6T, are shown in **Figure S7** for $LiCr(MoO_4)_2$ and β–$Li_{0.87}Na_{0.13}Cr(MoO_4)_2$ compound, respectively.

For both compounds, a weak hysteresis being more pronounced for β–$Li_{0.87}Na_{0.13}Cr(MoO_4)_2$ compound is observed. At this temperature (2K), the coercive magnetic field Hc was found equal to 11Oe and 75Oe; while remnant magnetization was estimated to 1.2 *m*emu/g and 4.5 *m*emu/g, for $LiCr(MoO_4)_2$ and β–$Li_{0.87}Na_{0.13}Cr(MoO_4)_2$, respectively. It is worthy notice that, at all studied magnetic field domain, the magnetization M varies almost linearly with H up to the highest measured field 6T, without showing any feature of meta-magnetic transition. Thus, measured magnetization reaches a value of only 2.91 emu/g ($0.20\mu_B$) and 3.08 emu/g ($0.21\mu_B$), for $LiCr(MoO_4)_2$ and β–$Li_{0.87}Na_{0.13}Cr(MoO_4)_2$ at H = 6T, respectively. They are far below the expected saturation magnetization Ms = $3\mu_B$ where (Ms = $gS\mu_B$, with g= 2 and S = 3/2). That clearly points out to the antiferromagnetic coupling in both compounds.

CONCLUSION

β–$Li_{0.87}Na_{0.13}Cr(MoO_4)_2$ compound has been synthesized as single crystal by solid-state reactions. Its structure has been determined by single crystal XRD. The Bond valence sum model (BVS) and charge distribution method (CHARDI) were used to confirm the structural model. This structure, isostructural to $LiCr(MoO_4)_2$, presents an open anionic framework facilitating ionic conductivity. The Rietveld refinement analyses of powder X-ray diffraction data have confirmed purity of the prepared powder materials. TGA/DTA thermal analysis shows no phase transition for the studied compound. As deduced from impedance spectroscopy and supported by BVEL calculations, the Na substitution of Li-site decrease the activation energy at high temperature, resulting a significant improvement in the ionic conductivity. In-situ High Temperature X-Ray Diffraction was used to study the thermal expansion of the studied material. Furthermore, the magnetic properties of both materials have been comparatively demonstrated using the field cooling squid measurements.

SUPPLEMENTARY MATERIAL

CCDC 1957397 contains the supplementary crystallographic data for and β–$Li_{0.87}Na_{0.13}Cr(MoO_4)_2$. These data can be obtained free of charge via www.ccdc.cam.ac.uk/data_request/cif, or by emailing data_request@ccdc.cam.ac.uk, or by contacting the Cambridge Crystallographic Data Centre, 12 Union Road, Cambridge CB2 1EZ, UK; fax: +44 1223 336033.

The figures and tables indicated by Figure S* and table S*, respectively, could be consulted in a supplementary file.

ACKNOWLEDGEMENTS

The authors wish to thank the Ministry of Higher Education and Scientific Research of Tunisia for the funding of the laboratory LMCTA LR15ES01.

The authors are greatly thankful to the UCA-PARTNER for the use of the Bruker SC single crystal diffractometer and the INKERMANN FUND, under the aegis of the Foundation de France, for the use of CMTC Anton Paar HTK1200N high temperature chamber.

AUTHORS E-MAIL ADDRESSES

sonni.manel@gmail.com,
faouzi.zid@fst.rnu.tn,
El-Kebir.Hlil@neel.cnrs.fr
Kader.Zaidat@grenoble-inp.fr
cecile.rossignol@lepmi.grenoble-inp.fr
Said.Obbade@phelma.grenoble-inp.fr

REFERENCES

[1] A.Sarapulova, D. Mikhailova, A. Senyshyn, H. Ehrenberg, Crystal structure and magnetic properties of Li,Cr-containing molybdates $Li_3Cr(MoO_4)_3$, $LiCr(MoO_4)_2$ and $Li_{1.8}Cr_{1.2}(MoO_4)_3$, J. Solid State Chem. 182 (2009) 3262-3268. https://doi.org/10.1016/j.jssc.2009.09.012

[2] J. Hanuza, M. Maczka, K. Hermanowicz, P.J. Deren, W. Strek, L. Folcik, H. Drulis, Spectroscopic Properties and Magnetic Phase Transitions in Scheelite $M^ICr(MoO_4)_2$ and Wolframite $M^ICr(WO_4)_2$ Crystals, where M^I=Li, Na, K, and Cs, J. Solid State Chem. 148 (1999) 468-478. https://doi.org/10.1006/jssc.1999.8482

[3] K. Feng, F. Wang, X. Yang, H. Zhang, X. Li, H. Zhang, $LiCr(MoO_4)_2$: a new high specific capacity cathode material for lithium ion batteries, J. Mater. Chem. A 7 (2019) 567-573. https://doi.org/10.1039/C8TA10274K

[4] C.N.R. Rao, A.K. Cheetham, Science and technology of nanomaterials: current status and future prospects. J. Mater. Chem. 11 (2001) 2887-2894. https://doi.org/10.1039/b105058n

[5] C. N. R. Rao, A. Müller, A. K. Cheetham (eds), WILEY-VCH Verlag GmbH & Co. KGaA, Weinheim 2004. https://doi.org/10.1007/s00396-004-1140-1

[6] Y.N. Xia, P.D. Yang, Y.G. Sun, Y.Y. Wu, B. Mayers, B. Gates, Y.D. Yin, F. Kim, Y.Q. Yan, One-Dimensional Nanostructures: Synthesis, Characterization, and Applications, Adv. Mater. 15 (2003) 353-389. https://doi.org/10.1002/adma.200390087

[7] L. Sebastian, Y. Piffard, A.K. Shukla, F. Taulellec, J. Gopalakrishnan, Synthesis, structure and lithium-ion conductivity of $Li_{2-2x}Mg_{2+x}(MoO_4)_3$ and $Li_3M(MoO_4)_3$ (M^{III} = Cr, Fe), J. Mater. Chem. 13 (2003) 1797–1802. https://doi.org/10.1039/b301189e

[8] I. Ennajeh, S. Georges, Y. Ben Smida, A. Guesmi, M.F. Zid, H. Boughzala, Synthesis, crystal structure, sintering and electrical properties of a new alluaudite-like triple molybdate $K_{0.13}Na_{3.87}MgMo_3O_{12}$, RSC Adv. 5 (2015) 38918-38925. https://doi.org/10.1039/c5ra02276b

[9] A.V.D. Lee, M. Beaurain, P. Armand, $LiFe(MoO_4)_2$, $LiGa(MoO_4)_2$ and $Li_3Ga(MoO_4)_3$, Acta Cryst. *C* 64 (2007) i1-i4. https://doi.org/10.1107/S0108270107061975

[10] A. Souilem, M.F. Zid, A. Driss, β-$Li_{0.37}Na_{0.63}Fe(MoO_4)_2$, Acta Cryst. *E* 70 (2014) i9-i10. https://doi.org/10.1107/S1600536814000646

[11] M. Sonni, M.F. Zid, C. Issaoui, Structural study, CHARDI and BVS validation and ionic migration pathways of a new lyonsite $(Na_{1/3}Li_{2/3})(Li_2,Cr)(MoO_4)_3$, J. Solid State Chem. 272 (2019) 244-248. https://doi.org/10.1016/j.jssc.2019.02.009

[12] N. Chen, Y. Yao, D. Wang, Y. Wei, X. Bie, C. Wang, G. Chen, F. Du, $LiFe(MoO_4)_2$ as a Novel Anode Material for Lithium-Ion Batteries, ACS Appl. Mater. Interfaces 6 (2014) 10661-10666. https://doi.org/10.1021/am502352c

[13] J. Gao, P. Zhao, K. Feng, $Na_{2.67}Mn_{1.67}(MoO_4)_3$: A 3.45 V Alluaudite-Type Cathode Candidate for Sodium-Ion Batteries, Chem. Mater. 29(3) (2017) 940-944. https://doi.org/10.1021/acs.chemmater.6b05308

[14] D. Du, R. Lan, K. Xie, H. Wang, S. Tao, Synthesis of $Li_2Ni_2(MoO_4)_3$ as a high-performance positive electrode for asymmetric supercapacitors, RSC Advances 7 (2017) 13304-13311. https://doi.org/10.1039/c6ra28580e

[15] K. Feng, F. Wang, H. Zhang, X. Li, H. Zhang, $Li_3Cr(MoO_4)_3$: a NASICON-type high specific capacity cathode material for lithium ion batteries, J. Mater. Chem. A 6 (2018) 19107-19112. https://doi.org/10.1039/C8TA07782G

[16] M. Alvarez-Vega, U. Amador, M.E. Arroyo-de Dompablo, Electrochemical Study of $Li_3Fe(MoO_4)_3$ as Positive Electrode in Lithium Cells, J. Electrochem. Soc. 152 (7) (2005) A1306-A1311. https://doi.org/10.1149/1.1925069

[17] J. Wang, G. Zhang, Z. Liu, H. Li, Y. Liu, Z. Wang, X. Li, K. Shih, L. Mai, $Li_3V(MoO_4)_3$ as a novel electrode material with good lithium storage properties and improved initial coulombic efficiency, Nano energy 44 (2017) 272-278. https://doi.org/10.1016/j.nanoen.2017.11.079

[18] A.A. Savina, V.A. Morozov, A.L. Buzlukov, I.Y. Arapova, S.Y. Stefanovich, Y.V. Baklanova, T.A. Denisova, N.I. Medvedeva, M. Bardet, J. Hadermann, B.I. Lazoryak, E.G. Khaikina, New Solid Electrolyte $Na_9Al(MoO_4)_6$: Structure and Na^+ Ion Conductivity, Chem. Mater. 29 (20) (2017) 8901-8913. https://doi.org/10.1021/acs.chemmater.7b03989

[19] J.G. Bazarova, A.V. Logvinova, B.G. Bazarov, Y.L. Tushinova, S.G. Dorzhieva, J. Temuujin, Synthesis of new triple molybdates $K_5RZr(MoO_4)_6$ (R = Al, Cr, Fe, In, Sc) in the K_2MoO_4-$R_2(MoO_4)_3$-$Zr(MoO_4)_2$ systems, their structure and electrical properties, J. Alloys Compd. 741 (2018) 834-839. https://doi.org/10.1016/j.jallcom.2018.01.208

[20] K.M. Hercule, Q. Wei, O.K. Asare, L. Qu, A.M. Khan, M. Yan, C. Du, W. Chen, L. Mai, Interconnected Nanorods–Nanoflakes $Li_2Co_2(MoO_4)_3$ Framework Structure with Enhanced Electrochemical Properties for Supercapacitors, Adv. Energy Mater. 5 (2015) 1500060. https://doi.org/10.1002/aenm.201500060

[21] X. Huang, H. Guo, B. Li, Eu^{3+}-activated $Na_2Gd(PO_4)(MoO_4)$: A novel high-brightness red-emitting phosphor with high color purity and quantum efficiency for white light-emitting diodes, J. Alloys Compd. 720 (2017) 29-38. https://doi.org/10.1016/j.jallcom.2017.05.251

[22] W.B. Li, D. Zhou, H.H. Xi, L.X. Pang, X. Yao, Structure, Infrared Reflectivity and Microwave Dielectric Properties of $(Na_{0.5}La_{0.5})MoO_4$–$(Na_{0.5}Bi_{0.5})MoO_4$ Ceramics, J. Am. Ceram. Soc. 99 (2016) 2083-2088. https://doi.org/10.1111/jace.14175

[23] Y. Liu, H. Zuo, J. Li, X. Shi, S. Ma, M. Zhao, K. Zhang, C. Wang, Hydrothermal synthesis and multicolor luminescence properties of Dy^{3+}/Eu^{3+} co-doped $KLa(MoO_4)_2$ phosphors, Ceram. Int. 42 (2016) 7781-7786. https://doi.org/10.1016/j.ceramint.2016.01.210

[24] A.A. Savina, V.V. Atuchin, S.F. Solodovnikov, Z.A. solodovnikova, A.S. Krylov, E.A. Maximovskiy, M.S. Molokeev, A.S. Oreshonkov, A.M. Pugachev, E.G. Khaikina, Synthesis, structural and spectroscopic properties of acentric triple molybdate $Cs_2NaBi(MoO_4)_3$, J. Solid State Chem. 225 (2015) 53-58. https://doi.org/10.1016/j.jssc.2014.11.023

[25] A. Guesmi, M. Nespolo, A. Driss, Synthesis, crystal structure and charge distribution of $Na_7As_{11}O_{31}$: An oxygen-deficient layered sodium arsenate, J. Solid State Chem. 179 (2006) 2466-2471. https://doi.org/10.1016/j.jssc.2006.04.010

[26] M. Nespolo, Chardi-it a Program to Compute Charge Distributions and Bond Valences in Non-molecular Crystalline Structures. *CRM2, University Henri Poincaré Nancy I, France*, 2001.

[27] M. Nespolo, G. Ferraris, G. Ivaldi, R. Hoppe, Charge distribution as a tool to investigate structural details. II. Extension to hydrogen bonds, distorted and hetero-ligand polyhedra, Acta Cryst. B57 (2001) 652–664. https://doi.org/10.1107/S0108768101009879

[28] Softbv web page by Pr.Stefan Adams. < http://www.softbv.net/>.

[29] I.D. Brown, The Chemical Bond in Inorganic Chemistry – The Bond Valence Model. *IUCr Monographs on Crystallography*, Vol. 12, Oxford University Press, 2002.

[30] M. Sale, M. Avdeev, 3DBVSMAPPER: a program for automatically generating bond-valence sum landscapes, J. Appl. Crystallogr. 45 (2012) 1054-1056. https://doi.org/10.1107/S0021889812032906

[31] K. Momma, F. Izumi, VESTA 3 for three-dimensional visualization of crystal, volumetric and morphology data, J. Appl. Crystallogr. 44 (2011) 1272–1276. https://doi.org/10.1107/S0021889811038970

[32] S. Adams, R.P. Rao, Understanding Ionic Conduction and Energy Storage Materials with Bond-Valence-Based Methods. In: Brown I., Poeppelmeier K. (eds) Bond Valences. Structure and Bonding, vol 158. Springer, Berlin, Heidelberg 2014. https://doi.org/10.1007/430_2013_137

[33] S. Adams, R.P. Rao, High power lithium ion battery materials by computational design, Phys. Status Solidi A 208 (2011) 1746-1753. https://doi.org/10.1002/pssa.201001116

[34] S. Adams, R.P. Rao, Modelling of Ion Transport in Solids with a General Bond Valence Based Force-Field, Atom Indonesia 36 (3) (2010) 95-104. https://doi.org/10.17146/aij.2010.30

[35] L.J. Farrugia, WinGX and ORTEP for Windows: an update. J. Appl. Crystallogr. 45 (2012) 849-854. https://doi.org/10.1107/S0021889812029111

[36] A.C.T. North, D.C. Phillips, F.S. Mathews, A semi-empirical method of absorption correction, Acta Cryst. A24 (1968) 351-359. https://doi.org/10.1107/S0567739468000707

[37] G.M. Sheldrick, A short history of SHELX, Acta Cryst. A 64 (2008) 112-122. https://doi.org/10.1107/S0108767307043930

[38] B.G. Bazarov, T.V. Namsaraeva, R.F. Klevtsova, A.G. Anshits, T.A. Vereshchagina, L.A. Glinskaya, K.N. Fedorov, Z.h.G. Bazarova, Growth and crystal structure of binary molybdate $CsFe(MoO_4)_2$, Kristall. 55(4) (2010) 634-636. https://doi.org/10.1134/S1063774510040097

[39] R.F. Klevtsova, Crystal structure of $NaFe(MoO_4)_2$, Dokl. Akad. Nauk SSSR 221(6) (1975) 1322-1325.

[40] J. Rodriguez-Carvajal, FULLPROF 2011: A graphic tool for powder diffraction. Version January 2011.

[41] A. Le Bail, H. Duroy, J.L. Fourquet, Ab-initio structure determination of $LiSbWO_6$ by X-ray powder diffraction. Mater. Res. Bull. 23(3) (1988) 447-452. https://doi.org/10.1016/0025-5408(88)90019-0

[42] D. Johnson, Zview version 3.1c. *Scribner Associates. Inc*. 1990-2007.

[43] I.M. Hodge, M.D. Ingram, A.R. West, Impedance and modulus spectroscopy of polycrystalline solid electrolytes, J. Electroanal. Chem. Interf. Electrochem. 74 (1976) 125-143. https://doi.org/10.1016/S0022-0728(76)80229-X

[44] R.J. Cava, E.A. Rietman, Ionic conductivity of β-AgI, Phys. Rev. B 30 (1984) 6896-6902. https://doi.org/10.1103/PhysRevB.30.6896

[45] H. Dhaouadi, O. Ghodbane, F. Hosni, F. Touati, Mn_3O_4 Nanoparticles: Synthesis, Characterization, and Dielectric Properties, *ISRN Spectroscopy*. (2012). https://doi.org/10.5402/2012/706398

[46] B.K. Barick, K.K. Mishra, A.K. Arora, R.N.P. Choudhary, D.K. Pradhan, Impedance and Raman spectroscopic studies of $(Na_{0.5}Bi_{0.5})TiO_3$, J. Phys. D Appl. Phys. 44 (2011) 355402. https://doi.org/10.1088/0022-3727/44/35/355402

[47] B. Lopez-Bermudez, W.G. Zeier, S. Zhou, A.J. Lehner, J. Hu, D.O. Scanlon, B.J. Morgan, B.C. Melot, Lithium-ion conductivity in $Li_6Y(BO_3)_3$: a thermally and electrochemically robust solid electrolyte, J. Mater. Chem. A 4 (2016) 6972-6979. https://doi.org/10.1039/C5TA09436D

[48] X. Li, X. Fan, Z. Xi, P. Liu, W. Long, P. Fang, F. Guo, R. Nan, Dielectric Relaxor and Conductivity Mechanism in Fe-Substituted PMN-32PT Ferroelectric Crystal, Cryst. 9 (2019) 241. https://doi.org/10.3390/cryst9050241